

Electronic Supplementary Information

Extremely lightweight and ultra-flexible infrared light converting quantum dot solar cells with high power-per-weight using a solution-processed bending durable silver nanowire electrode

Xiaoliang Zhang,^{a,b} * Viktor A. Öberg,^b Juan Du,^a Jianhua Liu,^a and Erik M. J. Johansson^b*

^a School of Materials Science and Engineering, Beihang University, Beijing 100191, China.

E-mail: xiaoliang.zhang@kemi.uu.se

^b Department of Chemistry-Ångström, Physical Chemistry, Uppsala University, 75120 Uppsala, Sweden.

E-mail: erik.johansson@kemi.uu.se

Content

S1. Supplementary Figures

Fig. S1. SEM images of the Ag NWs.

Fig. S2. Photographs of the Ag NW ink and glass/Ag NWs.

Fig. S3. Light transmittance spectra and resistance of the Ag NW electrode.

Fig. S4. The flexible PEN/Ag NWs adhered on a pre-stretched elastomer.

Fig. S5. Resistance of the PEN/Ag NWs on the glass/PDMS supporting substrate and pre-stretched elastomer.

Fig. S6. Schematically presentation of the fabrication of the flexible CQD solar cell.

Fig. S7. SEM image of the Ag NWs covered with AZO NP layer.

Fig. S8. Transmission spectra of the glass substrate covered with Ag NWs and Ag NWs/AZO.

Fig. S9. TEM image, absorption and photoluminescence spectrum of PbS CQDs.

Fig. S10. AFM image of AZO NP layer and PbS CQD solid layer.

Fig. S11. Cross-sectional SEM image of the traditional ITO-based CQD solar cell.

Fig. S12. Cross-sectional SEM image of the Ag NW-based CQD solar cell.

Fig. S13. *J-V* curves of the flexible CQD solar cell.

Fig. S14. *J-V* curves of the flexible CQD solar cell with different voltage scanning step.

Fig. S15. Integrated photocurrent density from the IPCE results.

Fig. S16. The flexible solar cell sticks to a pre-stretched elastomer.

Fig. S17. IPCE spectra of the CQD solar cell under compression.

Fig. S18. SEM image of the flexible CQD solar cell under 30% compression.

Fig. S19. SEM image of the flexible CQD solar cell re-stretched back to flat.

Fig. S20. *I-V* curves of the flexible CQD solar cell with cyclic compression-stretching.

Fig. S21. Photovoltaic metrics plotted at each 30% compression-stretching during 40 cycles of compression-stretching.

Fig. S22. IPCE spectra of the CQD solar cell after compression-stretching cycles.

Fig. S23. Device efficiency metrics plotted after 30% compression-stretching cycles in parallel to the Au electrode.

S2. Supplementary Tables

Table S1. Photovoltaic parameters and specific weight of different lightweight solar cells.

Table S2. Summarized photovoltaic performance of flexible quantum dot solar cells.

Table S3. Summarized photovoltaic performance of the solar cell with Ag NWs as a front electrode.

S3. Supplementary References

S1. Supplementary Figures

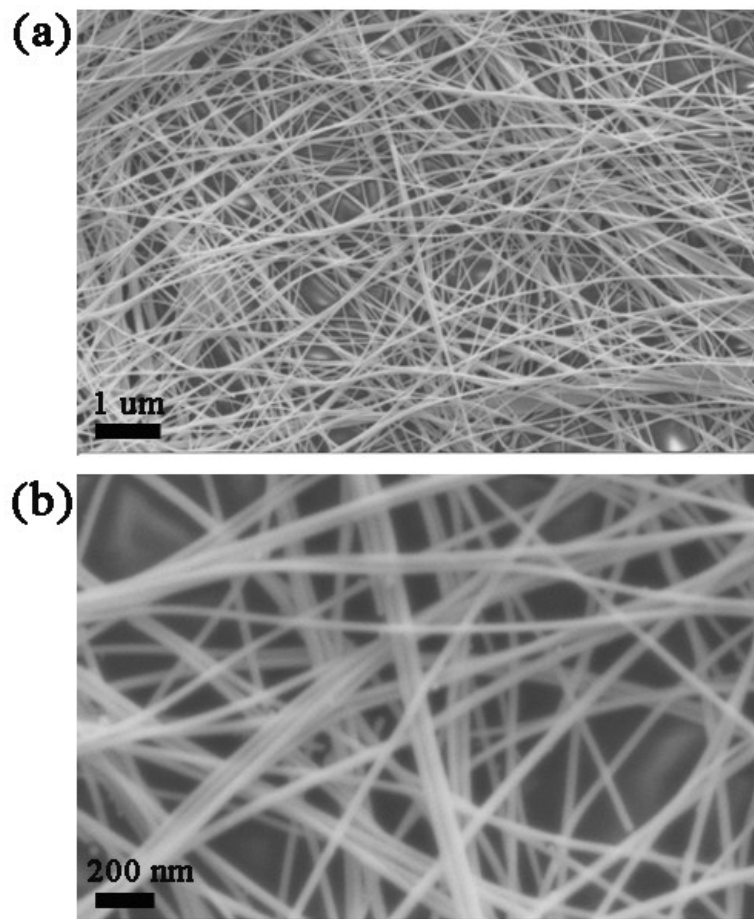


Fig. S1. (a) Low magnification and (b) high magnification SEM images of the Ag NWs. The Ag NW has a diameter of ~30 nm and length of 100-200 μm .

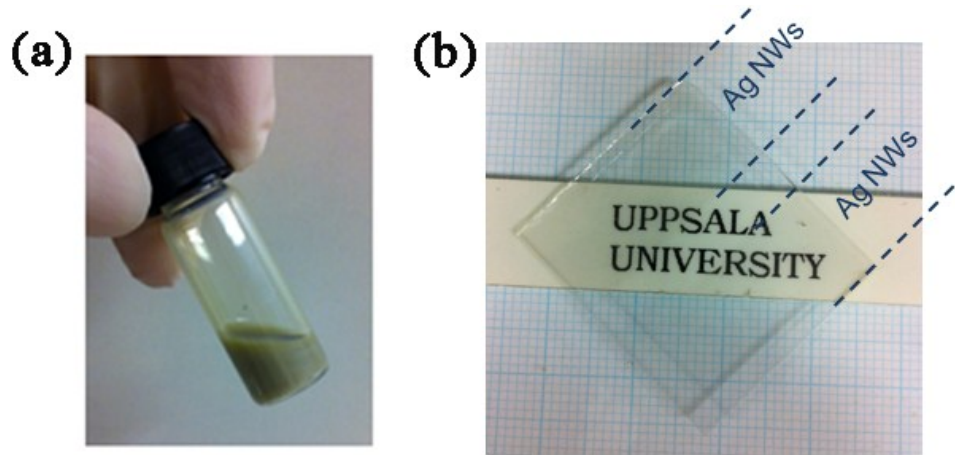


Fig. S2. (a) Photograph of the Ag NW ink and (b) the Ag NW network covered glass substrate. The Ag NW ink was spin-coated on the glass substrate under the ambient conditions. The middle part in the Ag NW network covered glass substrate was cleaned with cotton and then sintered at 150 °C for 20 min under nitrogen atmosphere.

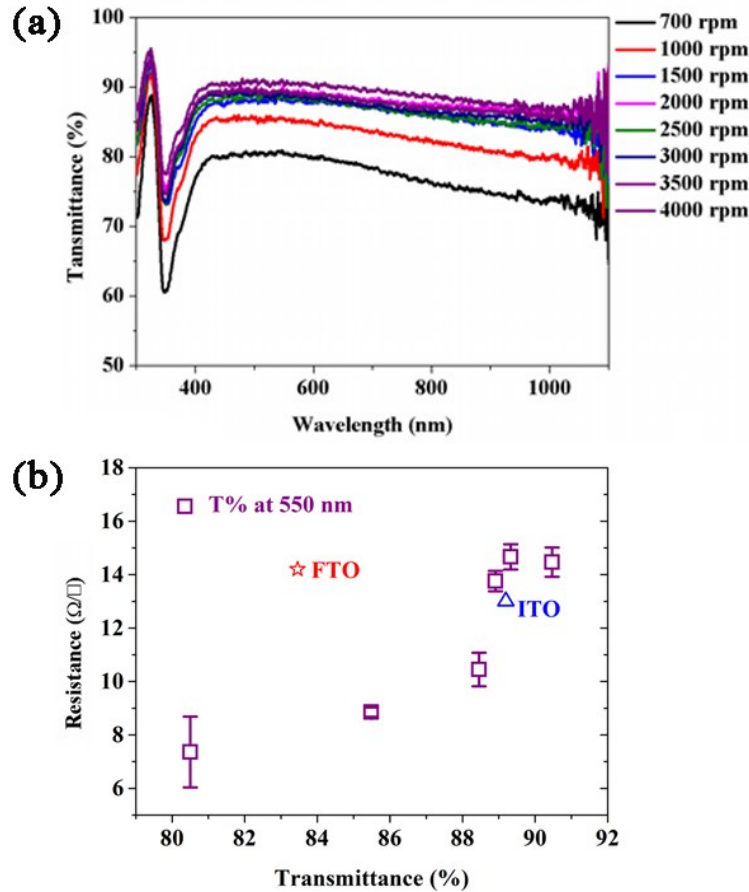


Fig. S3. (a) Transmittance spectra of the Ag NW networks prepared with different speed of spin-coating. (b) The resistance of the Ag NW networks as a function of the transmittance (@ 550 nm) of the Ag NW networks. The resistance was measured using four-point probe equipment in the area of $1.4 \times 1.4 \text{ cm}^2$ and more than 13 points were collected in such area for the statics. The FTO and ITO glass substrate were also tested and plotted in the figure for comparison. The results show that the transparent Ag NW network-based electrode has comparable or even better conductivity and transparency than the FTO or ITO-based electrode.

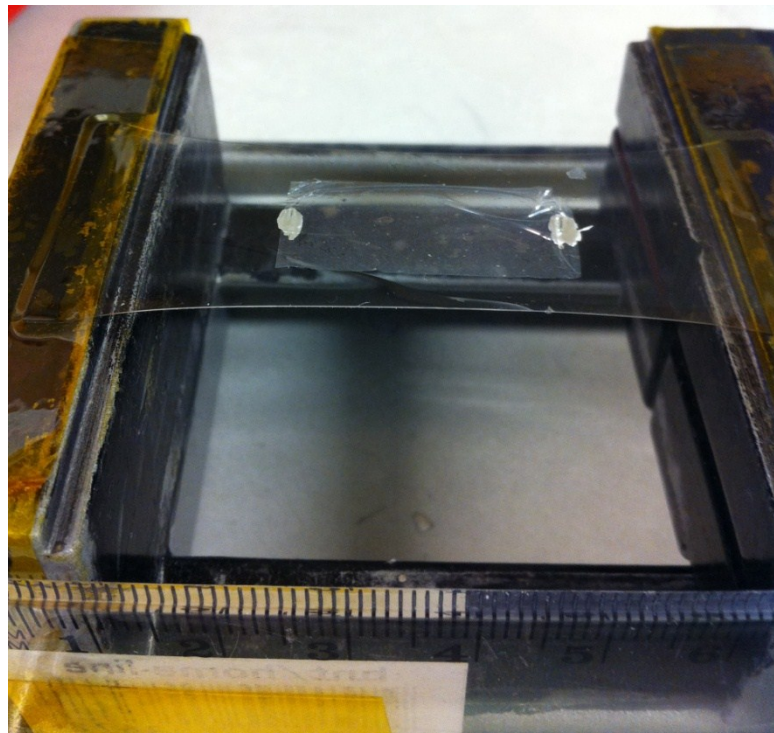


Fig. S4. The flexible PEN/Ag NW substrate is adhered on a pre-stretched elastomer to study the evolution of the conductivity with compression.



Fig. S5. Resistance of the PEN/Ag NW network on the (a) glass/PDMS supporting substrate and peeled away from the glass/PDMS and adhered on a pre-stretched elastomer. During transforming the PEN/Ag NW electrode no significant difference in the resistance was observed.

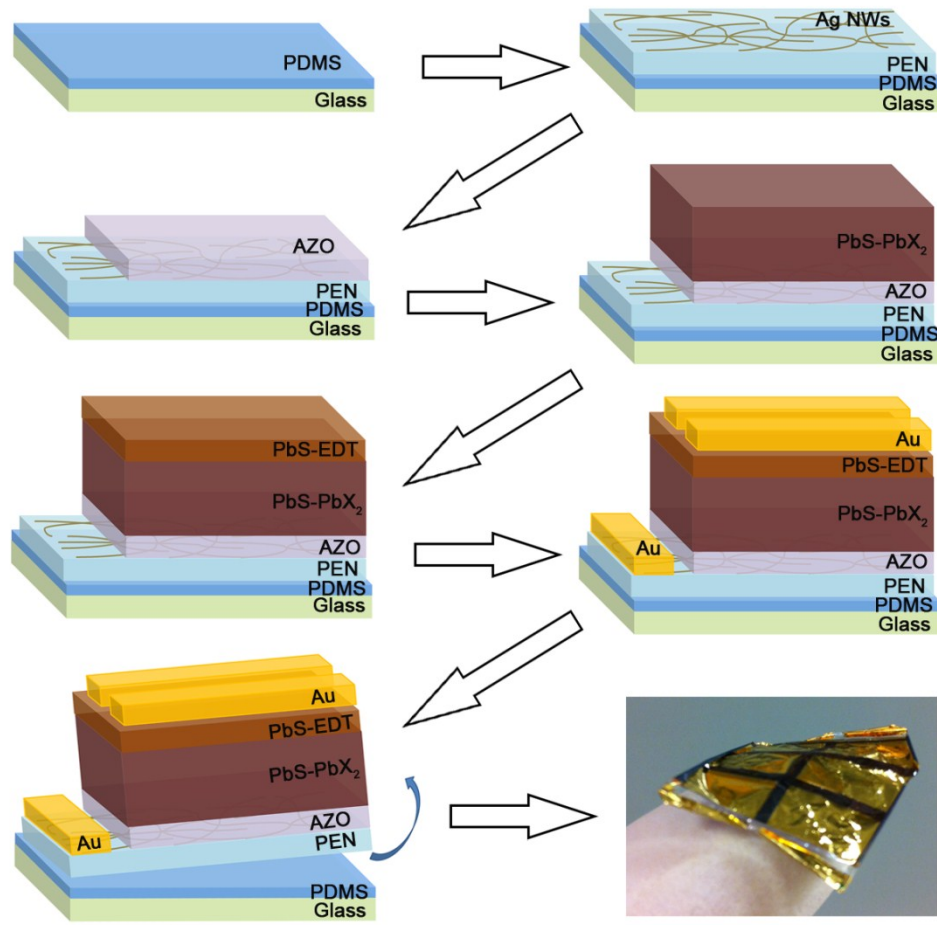


Fig. S6. Schematically present the fabrication processes of the flexible CQD solar cell. The glass/PDMS is used as a supporting substrate for the solar cell fabrication, such as spin-coating, annealing and Au deposition. After completed the device fabrication, the solar cell is peeled away from the glass/PDMS supporting substrate. Details are described in the Experimental section in the manuscript.

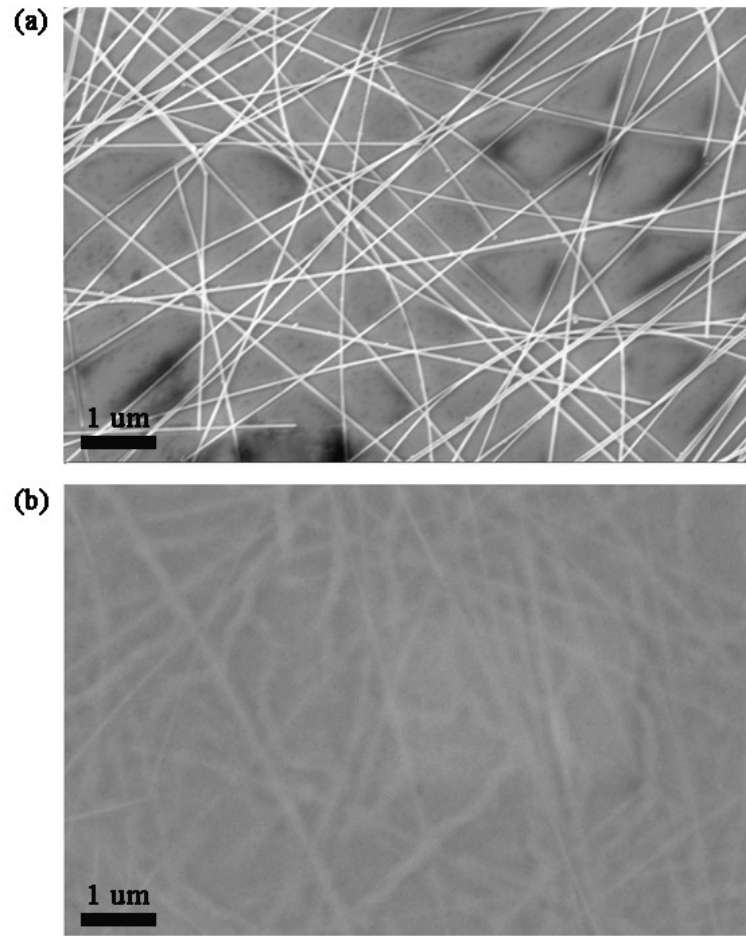


Fig. S7. SEM image of (a) the Ag NW network and (b) the network covered with AZO NP layer.

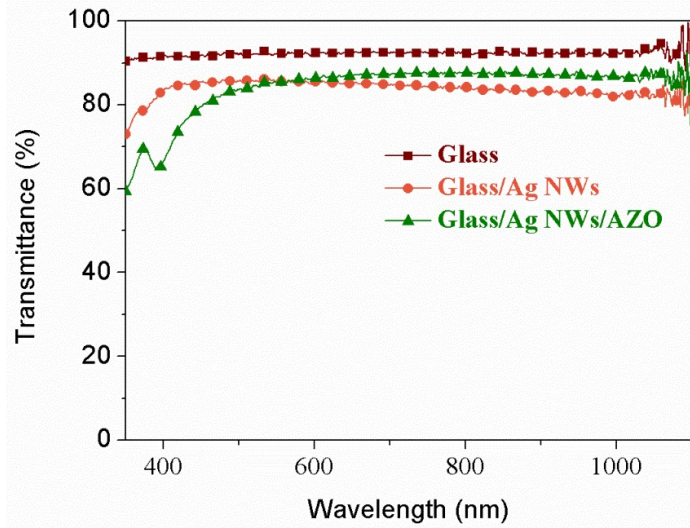


Fig. S8. Transmission spectra of the glass substrate covered with Ag NWs and Ag NWs/AZO.

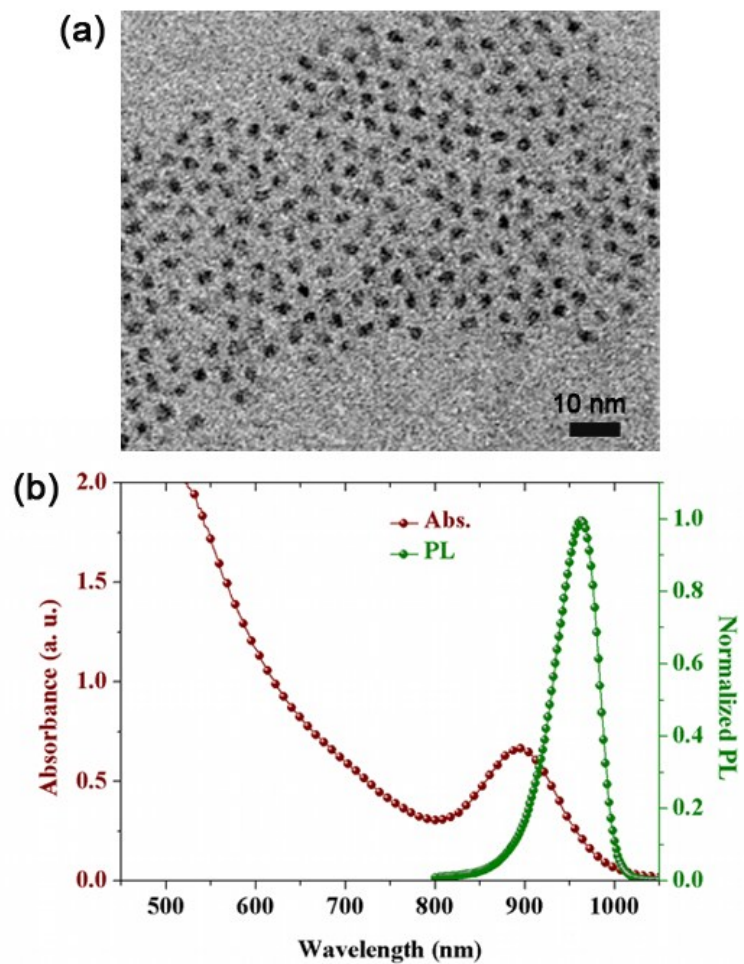


Fig. S9. (a) TEM image of PbS CQD capped by oleic acid. (b) Absorption and normalized photoluminescence spectra of PbS CQD.

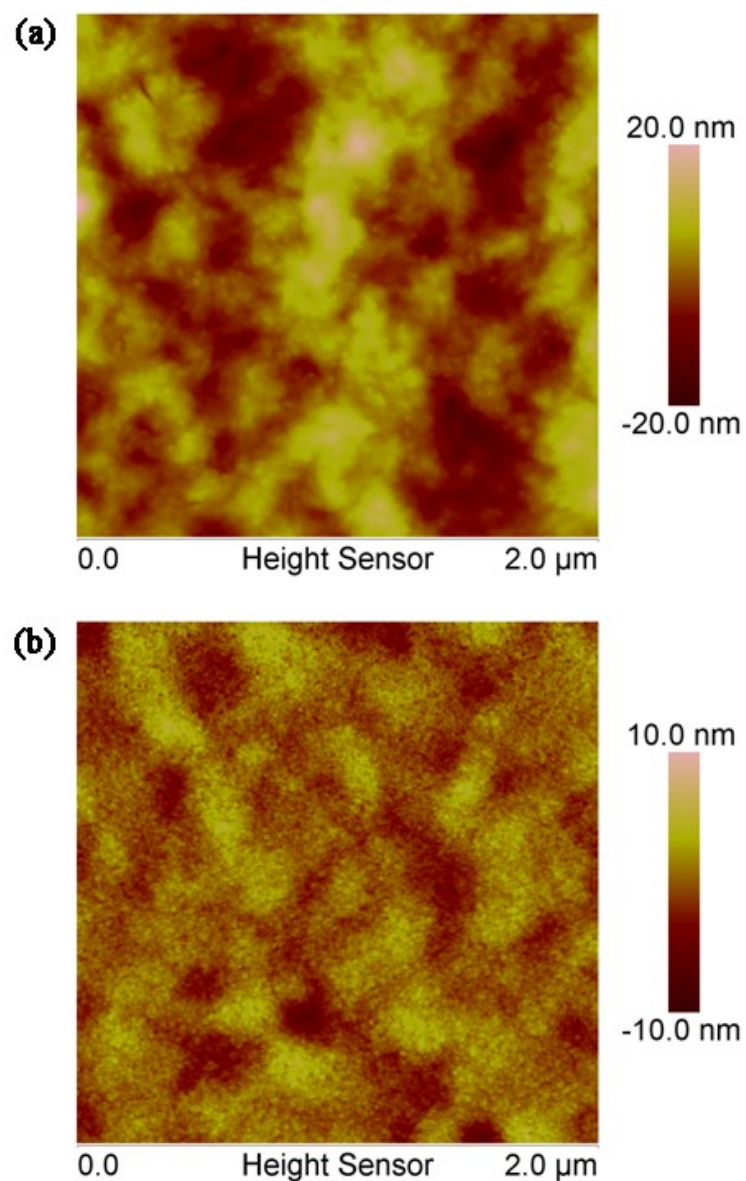


Fig. S10. AFM images of (a) the deposited AZO nanoparticle layer and (b) PbS CQD solid layer.

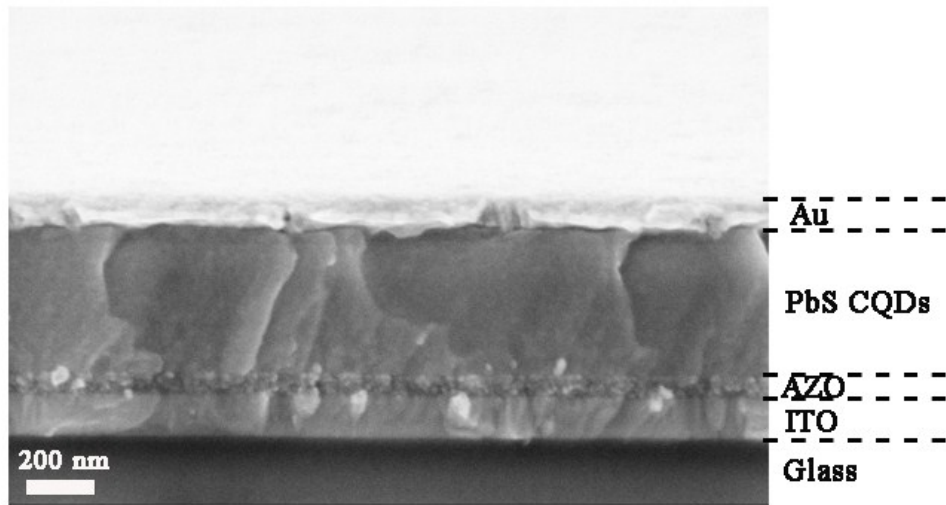


Fig. S11. Cross-sectional SEM image of the CQD solar cell fabricated on the traditional glass/ITO substrate.

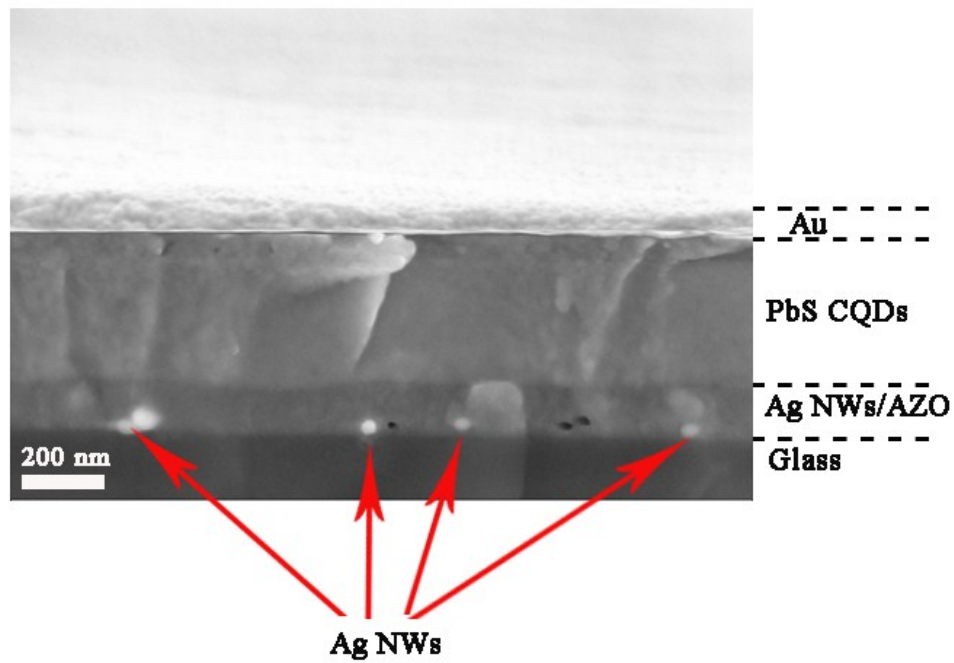


Fig. S12. Cross-sectional SEM image of the CQD solar cell fabricated on the glass substrate with the Ag NWs as front transparent electrode. The Ag NWs were draw out from the Ag NWs/AZO layer during cutting the sample for the measurement and left holes in the Ag NWs/AZO layer.

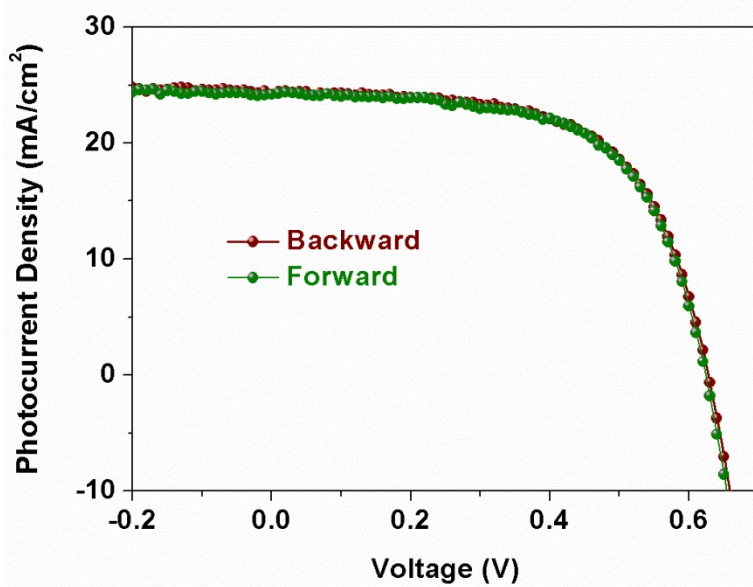


Fig. S13. J - V curves of the flexible CQD solar cell with Ag NWs as front electrode. The forward (from J_{sc} to V_{oc}) and backward (from V_{oc} to J_{sc}) scanning were performed for the measurements and no hysteresis is observed. The voltage step of 10 mV with a delay of 10 ms is applied to record the J - V curves.

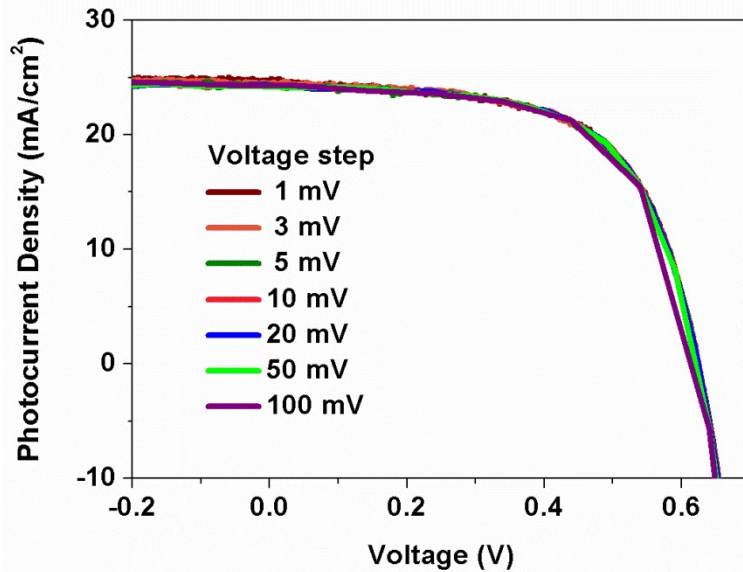


Fig. S14. *J-V* curves of the flexible CQD solar cell with different voltage scanning step. The voltage scanning step with a value of 1-100 mV and a delay of 10 ms were applied for the measurement. There is no noticeable difference when different voltage scanning step was applied for the measurement.

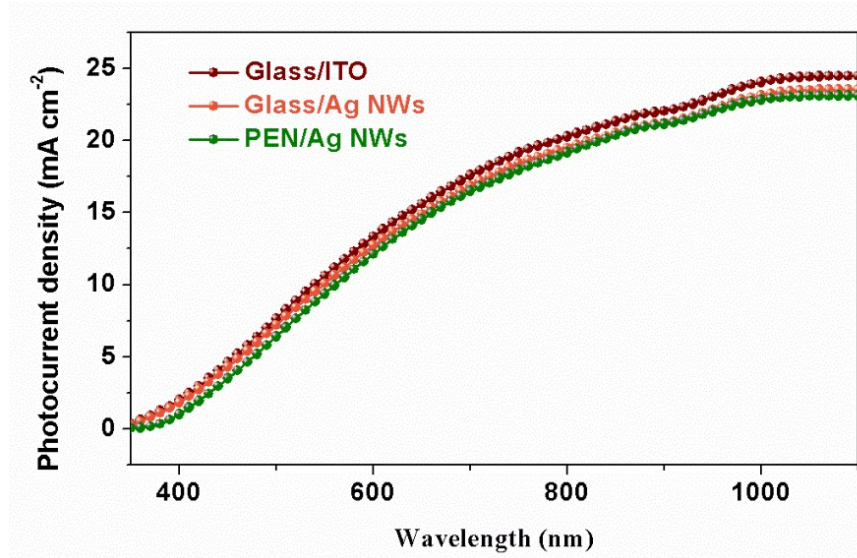


Fig. S15. Integrated photocurrent density from the IPCE results for the CQD solar cell with different substrate and front transparent electrode. The calculated photocurrent density is in good agreement with the photocurrent density measured from the *J-V* measurement.

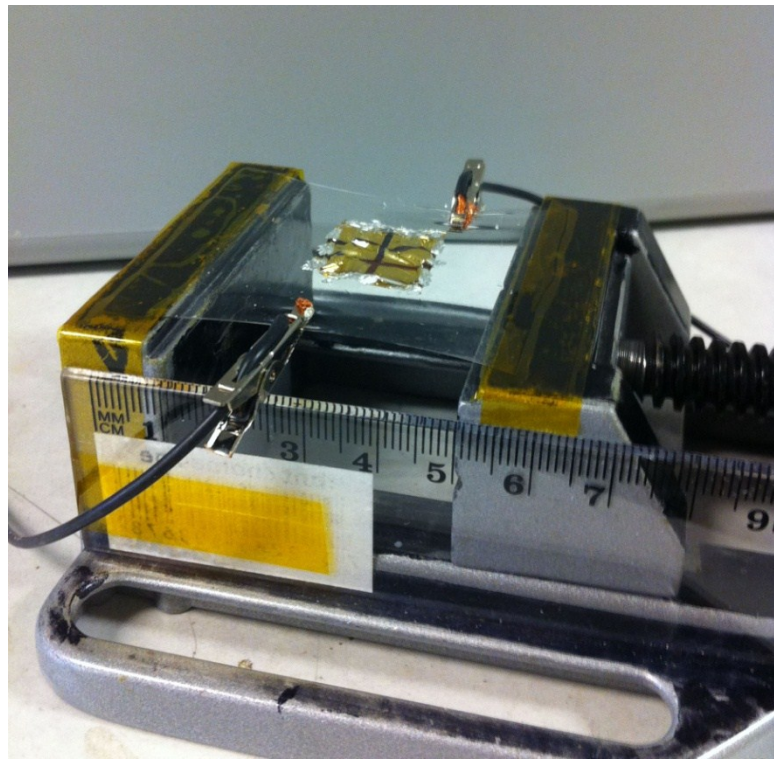


Fig. S16. The flexible CQD solar cell is stucked to a pre-stretched elastomer *via* wan der Walls bonding. The pre-stretched elastomer is slowly relaxing and the *I-V* curves are recorded under AM1.5G 100 mW cm⁻². For the cyclic compression-stretching measurement, the elastomer is repeated stretched and relaxed and then the *I-V* curves are recorded.

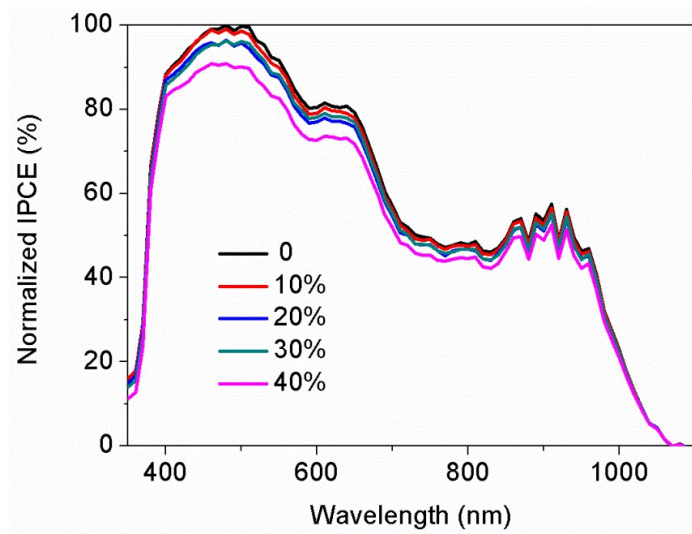


Fig. S17. IPCE spectra of the CQD solar cell under compression.

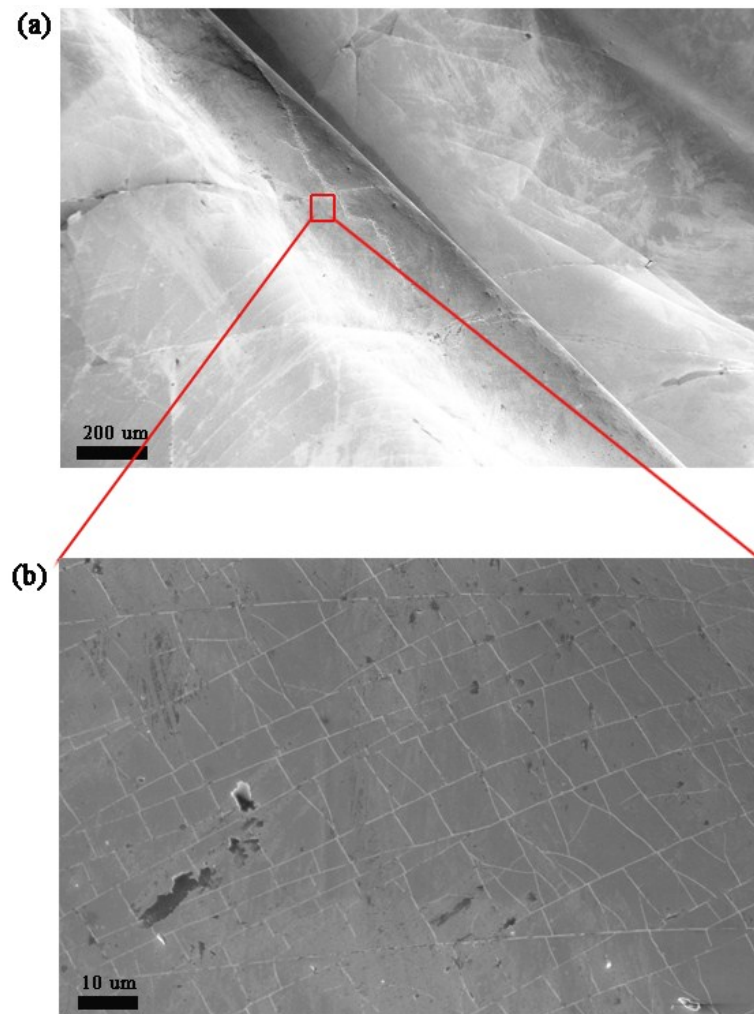


Fig. S18. (a) Low magnification and (b) high magnification SEM image of the flexible CQD solar cell under 30% compression.

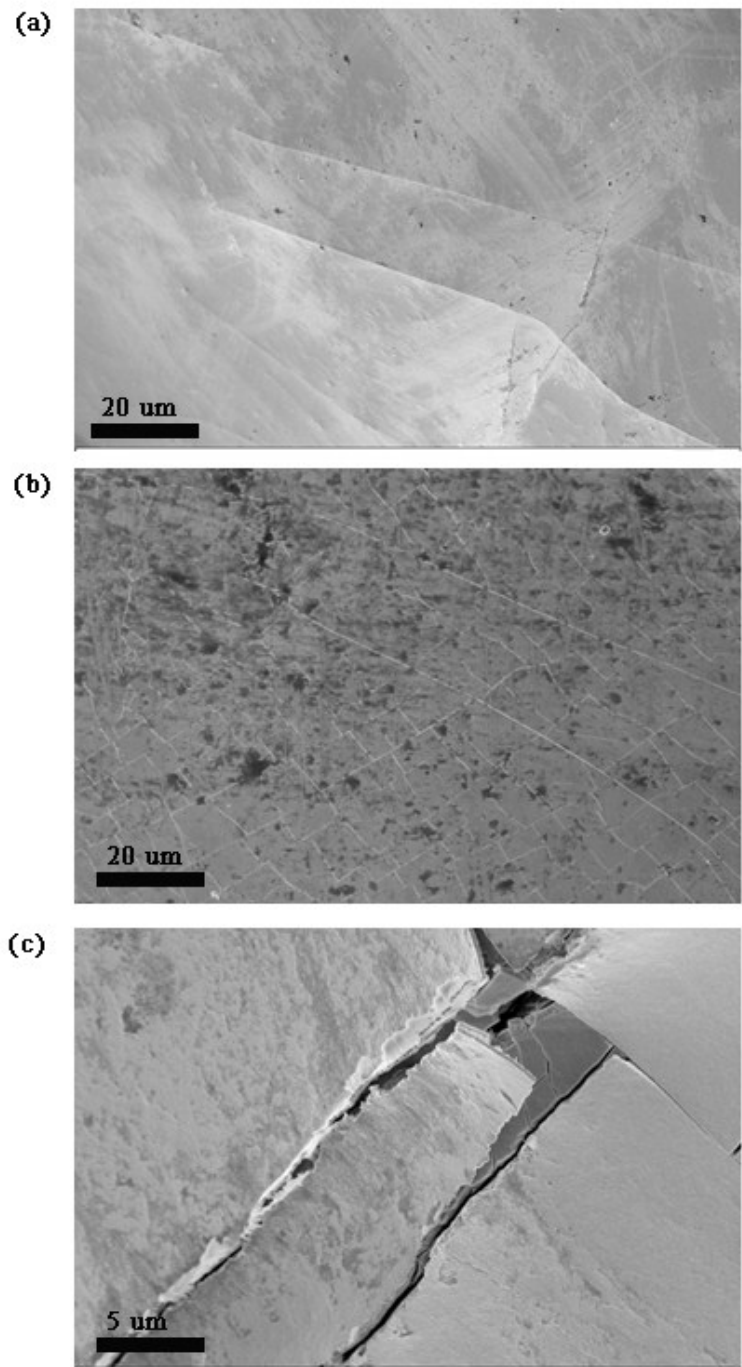


Fig. S19. SEM image of the flexible CQD solar cell re-stretched back to flat from (a) 10% compression, (b) 30% compression and (c) 60% compression.

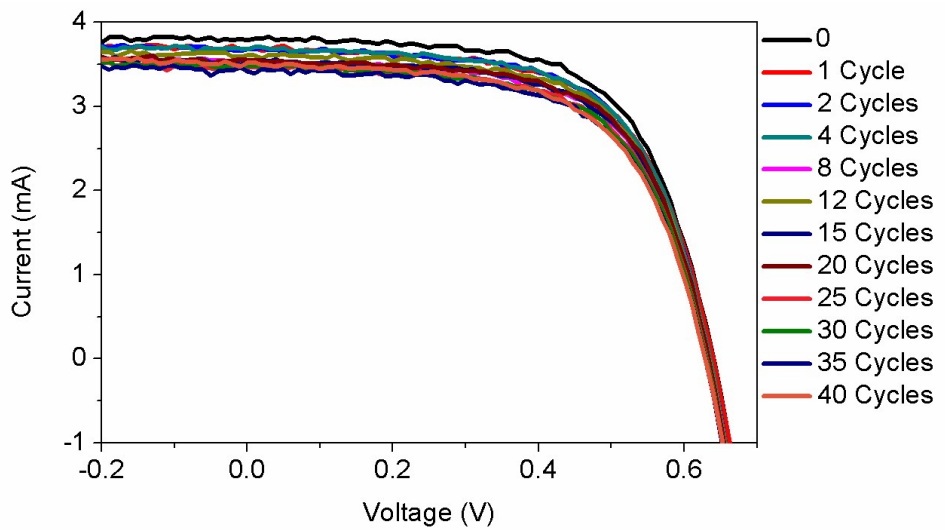


Fig. S20. I - V curves of the flexible CQD solar cell with cyclic compression-stretching.

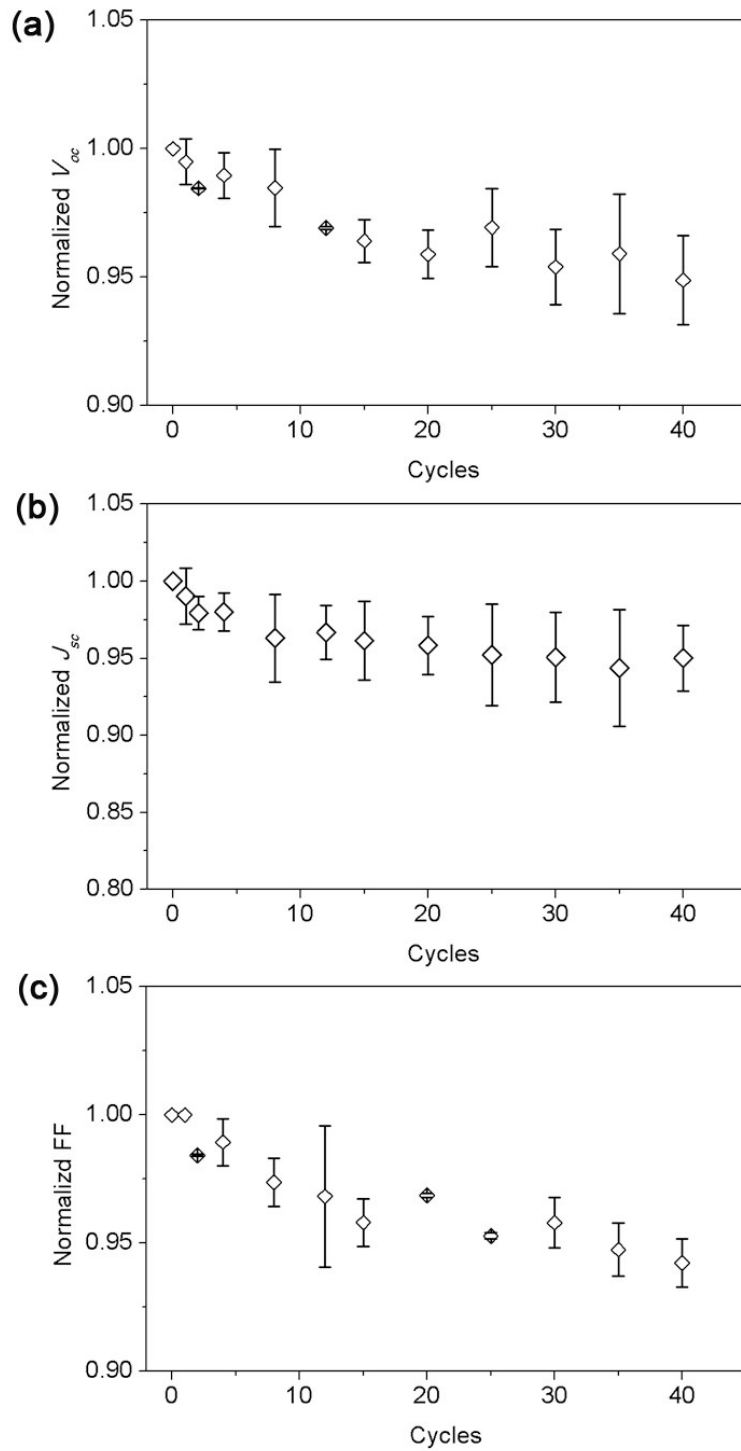


Fig. S21. (a) V_{oc} , (b) J_{sc} and (c) FF metrics plotted at each 30% compression-stretching during 40 cycles.

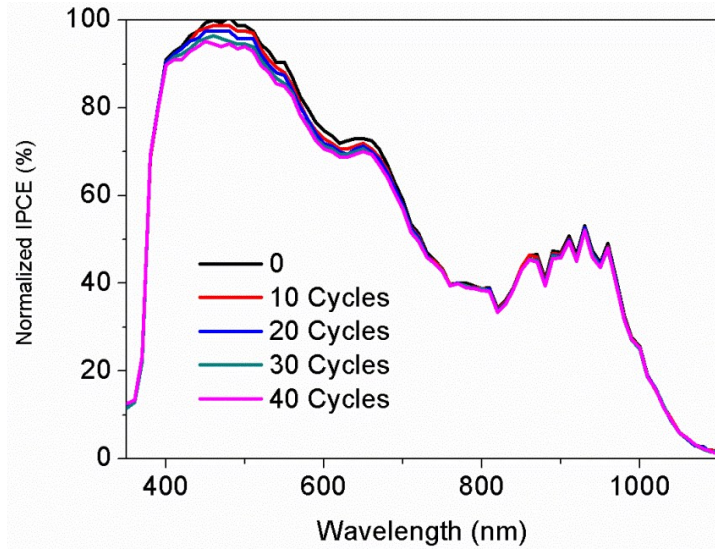


Fig. S22. IPCE spectra of the CQD solar cell under compression-stretching.

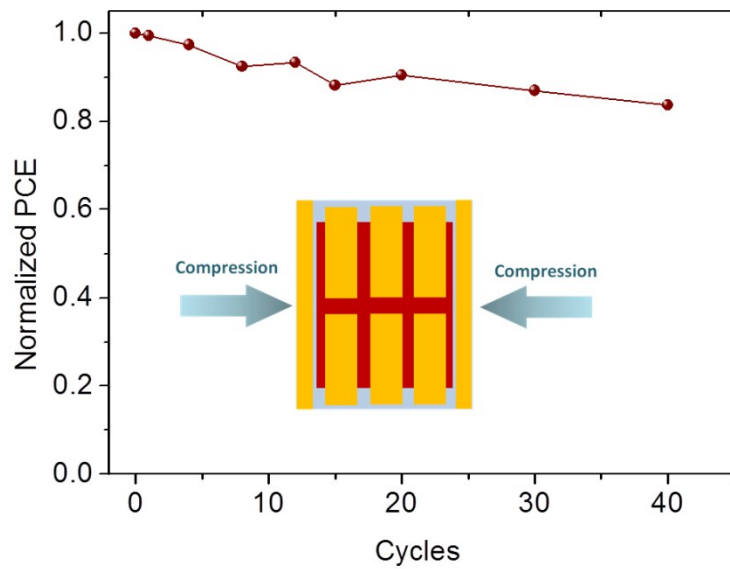


Fig. S23. Device efficiency metrics plotted at each 30% compression-stretching in parallel to the Au electrode.

S2. Supplementary Tables

Table S1. Photovoltaic parameters and specific weight of different lightweight solar cells.

Solar Cells	V_{oc}	J_{sc} (mA cm ⁻²)	FF	PCE	Specific Weight	Ref.
	(V)			(%)	(W g ⁻¹)	
PSC	0.926	17.6	0.73	11.9	22.88	1
a-Si/nc-Si	1.26	10.04	0.64	8.12	0.135	2,3
CdTe	0.765	20.9	0.71	11.4	2	4
CIGS PI	0.712	34.8	0.757	18.7	3.04-3.12	5
a-Si	0.888	14.3	0.7	8.8	0.125-0.957	6,7
InP	0.62	29.6	0.55	10.2	2	8
Poly-c Si	0.654	38.1	0.795	19.8	0.322	9
Mono-c Si	0.696	42.0	0.836	24.4	0.3965	9,10
3-mil Si	-	-	-	14.1	0.676	11
InGaP/GaAs	-	-	-	20.9	0.319	11
InGaP/GaAs/Ge	-	-	-	23.9	0.360	11
CIGS glass	0.712	36.1	0.779	20.04	0.0264	12
OSC	0.58	11.9	0.61	4	10	13
CQD	0.64	24.6	0.63	9.9	15.2	This work

Abbreviation: CIGS, copper indium gallium selenide; OSC, organic solar cell; PSC, perovskite solar cell.

Table S2. Summarized photovoltaic performance of flexible quantum dot solar cells.

Device structure	V_{oc} (V)	J_{sc} (mA cm ⁻²)	FF	PCE (%)	Ref.
PET/ITO/PbS-MPA/MoO₃/Au^{a)}	0.59	22.9	0.54	7.2	14
Ti/ZnO/CdS^{b)}	3.7	0.41	0.49	0.74	15
Ti/ZnO/ZnSe/CdSe^{b)}	0.64	15.3	0.53	5.1	16
Ni/TiO₂/CdSe^{b)}	0.58	9.9	0.61	3.6	17
Ti/ZnO/CdS/CdSe^{b)}	0.36	23.7	0.4	3.4	18
PET/ITO/ZnO/PbS-MPA/P₃HT/Au^{a)}	0.56	12.1	0.5	3.4	19
PET/SWCNTs/PEDOT:PSS/CQDs/PCBM/Ag	0.55	18.7	0.55	5.6	20
a)					
PET/MoO₃/Au/MoO₃/PbS-MPA/ZnO/Al^{a)}	0.59	19.5	0.59	6.8	21
ZnO/CdSe^{b)}	0.58	2.70	0.47	0.74	22
PET//ITO/MZO/PbS-TBAI/PbS-EDT/Au^{a)}	0.62	24.5	0.62	9.4	23
PEN/Ag NWs/AZO/PbS-PbX₂/PbS-EDT/Au^{a)}	0.64	24.6	0.63	9.9	This work

^{a)} Heterojunction colloidal quantum dot solar cell^{b)} Sensitized quantum dot solar cell

Table S3. Summarized photovoltaic performance of the solar cell with Ag NWs as front transparent electrode.

Device	V_{oc} (V)	J_{sc} (mA cm $^{-2}$)	FF	PCE %)	Ref.
OSC	0.75	8.6	0.39	2.5	24
	0.77	17.9	0.65	8.8	25
	0.67	13.1	0.57	5.2	26
	0.59	19.5	0.59	6.8	21
	-	1.54	-	0.38	27
	0.46	2.91	0.60	1.1	28
	-	8.37	-	1.9	29
	0.44	7.20	0.43	1.3	30
	0.55	7.7	0.61	2.6	31
	0.59	8.6	0.46	2.4	32
DSSC	0.76	10.7	0.53	4.3	33
	0.71	10.45	0.41	3.04	34
	0.76	17.83	0.64	8.57	35
	0.76	15.1	0.65	7.4	36
Si	-	9.7	0.69	4.6	37
	0.59	24.5	0.4	5.7	38
PSC	0.96	13.2	0.39	4.9	39
	0.92	16.5	0.49	7.5	40
CQD	0.64	24.6	0.63	9.9	This work

S3. Supplementary References

- 1 M. Kaltenbrunner, G. Adam, E. D. Glowacki, M. Drack, R. Schwodiauer, L. Leonat, D. H. Apaydin, H. Groiss, M. C. Scharber, M. S. White, N. S. Sariciftci and S. Bauer, *Nat. Mater.*, 2015, **14**, 1032-1039.
- 2 Nuon Endless energy from solar foil [Brochure] (2009). Retrieved from <https://www.bnr.nl/binaries/1000/10/47/helianthos-brochure-tcm164-66850.pdf>
- 3 J. K. Rath, M. Brinza, Y. Liu, A. Borreman and R. E. I. Schropp, *Sol. Energ. Mat. Sol. Cells*, 2010, **94**, 1534-1541 .
- 4 A. Romeo, G. Khrypunov, F. Kurdesau, M. Arnold, D. L. Bätzner, H. Zogg and A. N. Tiwari, *Sol. Energ. Mat. Sol. Cells*, 2006, **90**, 3407-3415.
- 5 A. Chirilă, S. Buecheler, F. Pianezzi, P. Bloesch, C. Gretener, A. R. Uhl, C. Fella, L. Kranz, J. Perrenoud, S. Seyrling, R. Verma, S. Nishiwaki, Y. E. Romanyuk, G. Bilger and A. N. Tiwari, *Nat. Mater.*, 2011, **10**, 857-861.
- 6 T. Söderström, F.-J. Haug, V. Terrazzoni-Daudrix and C. Ballif, *J. Appl. Phys.*, 2008, **103**, 114509 .
- 7 Fraunhofer FEP Rolle-zu-rolle-anlage für OLED und OPV [Brochure]. Retrieved from Https://www.fep.fraunhofer.de/content/dam/fep/de/documents/Anlagenflyer/M06_Rolle-zu-Rolle-Anlage%20f%C3%BCr%20OLED%20und%20OPV_DE_net.pdf
- 8 K.-T. Shiu, J. Zimmerman, H. Wang and S. R. Forrest, *Appl. Phys. Lett.*, 2009, **95**, 223503.
- 9 J. Zhao, A. Wang, M. A. Green and F. Ferrazza, *Appl. Phys. Lett.*, 1998, **73**, 1991-1993.
- 10 J. Zhao, A. Wang, P. Altermatt and M. A. Green, *Appl. Phys. Lett.*, 1995, **66**, 3636-3638.
- 11 N. S. Fatemi, H. E. Pollard, H. Q. Hou and P. R. Sharps, *Conference Record of the Twenty-Eighth IEEE Photovoltaic Specialists Conference*, 2000, 1083-1086 .
- 12 P. Jackson, D. Hariskos, E. Lotter, S. Paetel, R. Wuerz, R. Menner, W. Wischmann and M. Powalla, *Prog. Photovolt. Res. Appl.*, 2011, **19**, 894-897.

- 13 M. Kaltenbrunner, M. S. White, E. D. Głowacki, T. Sekitani, T. Someya, N. S. Sariciftci
and S. Bauer, *Nat. Commun.*, 2012, **3**, 770 .
- 14 I. J. Kramer, G. Moreno-Bautista, J. C. Minor, D. Kopilovic and E. H. Sargent, *Appl. Phys.
Lett.*, 2014, **105**, 163902.
- 15 H. Liu, G. Zhang, J. Liang, J. Li, J. Yang, J. Wei, W. Sun and Z. Shen, *IEEE J. Photovolt.*,
2016, **6**, 952-959.
- 16 Z. Du, M. Liu, Y. Li, Y. Chen and X. Zhong, *J. Mater. Chem. A*, 2017, **5**, 5577-5584.
- 17 Z. Du, J. Tong, W. Guo, H. Zhang and X. Zhong, *J. Mater. Chem. A*, 2016, **4**, 11754-11761.
- 18 Y. Li, L. Wei, C. Wu, C. Liu, Y. Chen, H. Liu, J. Jiao and L. Mei, *J. Mater. Chem. A*, 2014,
2, 15546-15552.
- 19 X. Zhang, J. Zhang, J. Liu and E. M. Johansson, *Nanoscale*, 2015, **7**, 11520-11524.
- 20 X. Zhang, K. Aitola, C. Hagglund, A. Kaskela, M. B. Johansson, K. Sveinbjornsson, E. I.
Kauppinen and E. M. Johansson, *ChemSusChem*, 2017, **10**, 434-441.
- 21 X. Zhang and E. M. J. Johansson, *Nano Energy*, 2016, **28**, 71-77.
- 22 J. Chen, W. Lei, C. Li, Y. Zhang, Y. Cui, B. Wang and W. Deng, *Phys. Chem. Chem. Phys.*,
2011, **13**, 13182-13184.
- 23 X. Zhang, P. K. Santra, L. Tian, M. B. Johansson, H. Rensmo and E. M. J. Johansson, *ACS
Nano*, 2017, **11**, 8478-8487.
- 24 L. Yang, T. Zhang, H. Zhou, S. C. Price, B. J. Wiley and W. You, *ACS Appl. Mater.
Interfaces*, 2011, **3**, 4075-4084.
- 25 J. H. Seo, I. Hwang, H. D. Um, S. Lee, K. Lee, J. Park, H. Shin, T. H. Kwon, S. J. Kang and
K. Seo, *Adv. Mater.*, 2017, **29**, 1701479.
- 26 M. Song, D. S. You, K. Lim, S. Park, S. Jung, C. S. Kim, D.-H. Kim, D.-G. Kim, J.-K. Kim,
J. Park, Y.-C. Kang, J. Heo, S.-H. Jin, J. H. Park and J.-W. Kang, *Adv. Funct. Mater.*, 2013,
23, 4177-4184.
- 27 J. Y. Lee, S. T. Connor, Y. Cui and P. Peumans, *Nano Lett.*, 2008, **8**, 689-692.

- 28 J. Y. Lee, S. T. Connor, Y. Cui and P. Peumans, *Nano Lett.*, 2010, **10**, 1276-1279.
- 29 T. Tokuno, M. Nogi, M. Karakawa, J. Jiu, T. T. Nge, Y. Aso and K. Suganuma, *Nano Res.*, 2011, **4**, 1215-1222.
- 30 D. Wang, W. Zhou, H. Liu, Y. Ma and H. Zhang, *Nanotechnology*, 2016, **27**, 335203.
- 31 K.-H. Choi, J. Kim, Y.-J. Noh, S.-I. Na and H.-K. Kim, *Sol. Energ. Mat. Sol. C.*, 2013, **110**, 147-153.
- 32 F. S. F. Morgenstern, D. Kabra, S. Massip, T. J. K. Brenner, P. E. Lyons, J. N. Coleman and R. H. Friend, *Appl. Phys. Lett.*, 2011, **99**, 183307.
- 33 P. Maisch, K. C. Tam, L. Lucera, H.-J. Egelhaaf, H. Scheiber, E. Maier and C. J. Brabec, *Org. Electron*, 2016, **38**, 139-143.
- 34 Y. Zhao, W. Zou, H. Li, K. Lu, W. Yan and Z. Wei, *Chin. J. Polym. Sci.*, 2016, **35**, 261-268.
- 35 S. Kang, T. Kim, S. Cho, Y. Lee, A. Choe, B. Walker, S. J. Ko, J. Y. Kim and H. Ko, *Nano Lett.*, 2015, **15**, 7933-7942.
- 36 H. Yan, J. Wang, B. Feng, K. Duan and J. Weng, *Solar Energy*, 2015, **122**, 966-975.
- 37 M. W. Khan, Asim and S. Kazmi, *IJIREEICE*, 2016, **4**, 176-181.
- 38 P. Aurang, D. Doganay, A. Bek, R. Turan and H. E. Unalan, *Solar Energy*, 2017, **141**, 110-117.
- 39 K. Yang, F. Li, J. Zhang, C. P. Veeramalai and T. Guo, *Nanotechnology*, 2016, **27**, 095202.
- 40 M. Lee, Y. Ko, B. K. Min and Y. Jun, *ChemSusChem*, 2016, **9**, 31-35.